Python workflow for segmenting multiphase flow in porous rocks

Catherine Spurin[1], Sharon Ellman[2], Dane Sherburn[3], Tom Bultreys[2], and Hamdi Tchelepi[1]

[1]Department of Energy Science & Engineering, Stanford University
[2]Department of Geology, Ghent
[3]Stanford Existential Risk Initiative, Stanford University

This work has not yet undergone peer review. We welcome any feedback and/ or comments.

Corresponding author: Catherine Spurin, cspurin@stanford.edu

Abstract

The need for accurate, consistent and fast image processing has become an important part of the investigation of multiphase flow through porous media. We describe an open-source image processing workflow written in python, using the sci-kit toolbox. We demonstrate the methodology to segment multiple fluids (gas and brine), and the rock grains for a Bentheimer sandstone. This workflow can be adapted to many applications.

1 Introduction

Recent advances in X-ray tomography has revolutionized the field of porous media research, by enabling the *in-situ* visualization of multiple fluid phases within the pore space of rocks (Wildenschild & Sheppard, 2013; Blunt, 2017). The underlying physics governing fluid flow has been explored using synchrotron tomography (Scanziani et al., 2020; Berg et al., 2013; Spurin et al., 2020), and fast lab-based micro computed tomography (Micro-CT) (Bultreys et al., 2016; Mascini et al., 2021; Bultreys et al., 2022). These findings are important in subsurface applications such as CO_2 storage (Garing et al., 2017) and hydrogen storage (Zhang et al., 2023), as examples.

Consequently, large amounts of 4D data has been generated that has to be segmented into the various fluid phases occupying the pore space, and the rock grains themselves. Segmentation is essential for quantitatively analyzing flow in porous media. However, segmentation can be a difficult and time-consuming process. The key issues for our field are: (1) the lack of ground truth data, (2) image artefacts, (3) features below or near the image resolution, and (4) difficulty in deciding a metric for segmentation. To address these issues, images can be filtered, we can only analyze features above the image resolution (a valid thing to do when looking at the non-wetting phase, which should occupy the largest pores (Spurin et al., 2020)), and implement more sophisticated methods such as machine learning, which potentially include more subtle features such as texture (while typical segmentation is done using image greyscale values) (Arganda-Carreras et al., 2017; Garfi et al., 2020) or super resolution (Zhou et al., 2022).

A range of image processing workflows exists, with many researchers opting for commercial software such as Avizo. However, using commercial software makes the results harder to reproduce, and it is more difficult to adapt the workflow specifically for flow in porous media. As a result, there are large variations and inconsistency between groups, which are not assessed when comparisons are made between the final segmented results. This creates a barrier to overcoming the key issues with segmentation in our field.

Our aim is to have accurate, consistent and fast image processing that anyone can use. Here we present a workflow for image segmentation using the sci-kit toolbox and python, that is specific to the porous media community. This workflow can be adapted or automated for a given application.

2 Python Workflow

We have two different workflows: (1) segmentation of the pore space, and (2) segmentation of the fluids within the pore space. The workflow for the segmentation of the pore space is discussed in Section 3, and the segmentation of the fluids is discussed in Section 4. A schematic of the workflow is shown in Figure 1. The workflow presented in this work requires a high quality scan of the sample without brine in the pore space for the pore space segmentation. This image can be acquired with air or deionized water occupying the pore space. We recommend deionized water pressurised to experimental conditions to minimise grain movement during the experiment. The flow image segmentation relies on subtracting the image with both fluids present, with an image where the sample is fully saturated with the wetting phase (referred to as the brine scan in Fig-

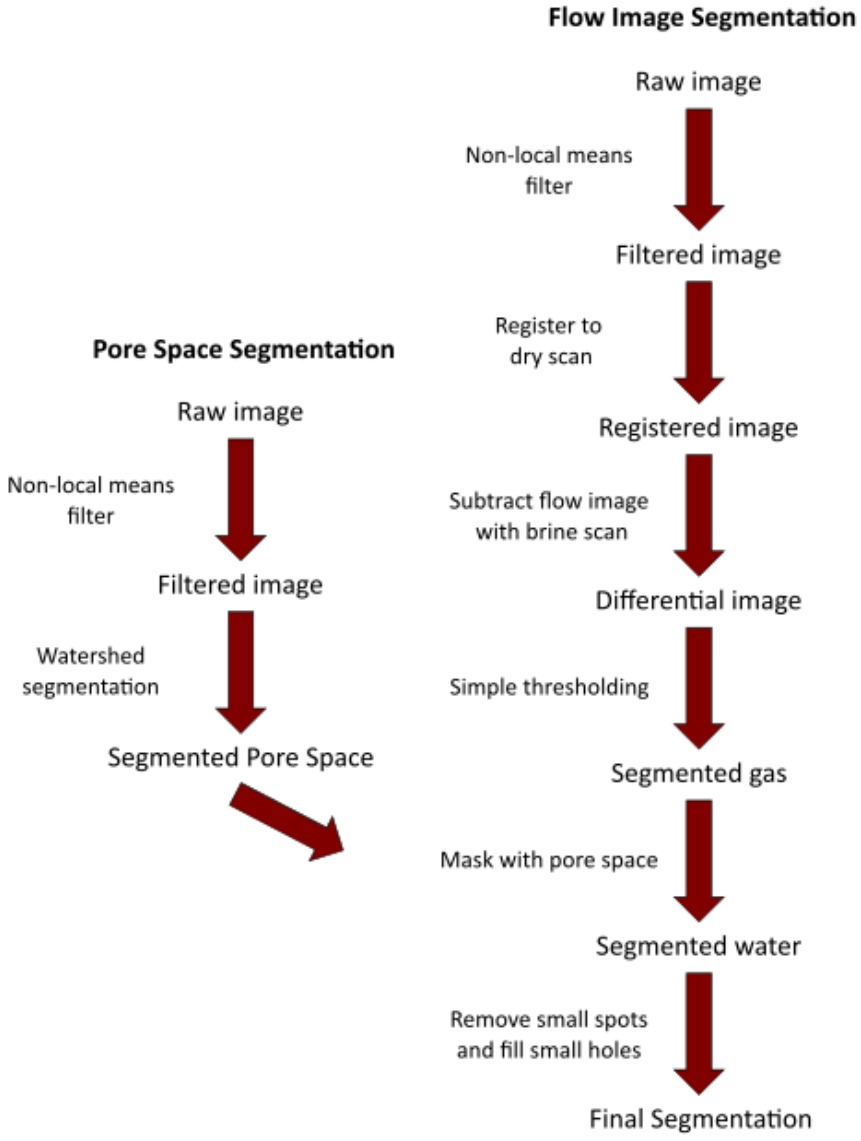

Figure 1. Image processing workflow for segmentation. The pore space segmentation requires a high quality image of the sample without brine present, as brine is highly attenuating. The segmentation of the flow images requires the segmented pore space, the image of the sample with both fluids present, and an image with just the wetting phase (typically brine) present.

ure 1). This is the easiest way to automate the segmentation process, as the subtraction leads to one peak in the greyscale histogram of the pore space, and makes segmentation more robust in instances where the fluid contrast is less extreme. The subtraction step can be removed if no brine scan was taken, and the contrast of the fluids is sufficient.

All images are loaded and transformed into an array prior to any processing. This was found to be the best representation of a large 3D data set for subsequent processing. All processing described within was performed on a desktop computer. There are

two notebooks for processing: (1) image_segmentation_3D for the segmentation of the pore space, and (2) flow_segmentation_3D for the segmentation of the fluids. A separate python package, utils, provides functions to load in and normalize images, and a visualisation to quality check the segmentation process.

3 Segmentation of the Pore Space

3.1 Filtering using a non-local means filter

The raw image is first filtered with a non-local means filter. This filter reduces noise, while maintaining boundaries between fluid phases (Buades et al., 2011). This is done by selecting a small patch of voxels, and comparing the voxel of interest to its surrounding neighbours; if the pixels have similar greyscale values, they are averaged, thus reducing noise.

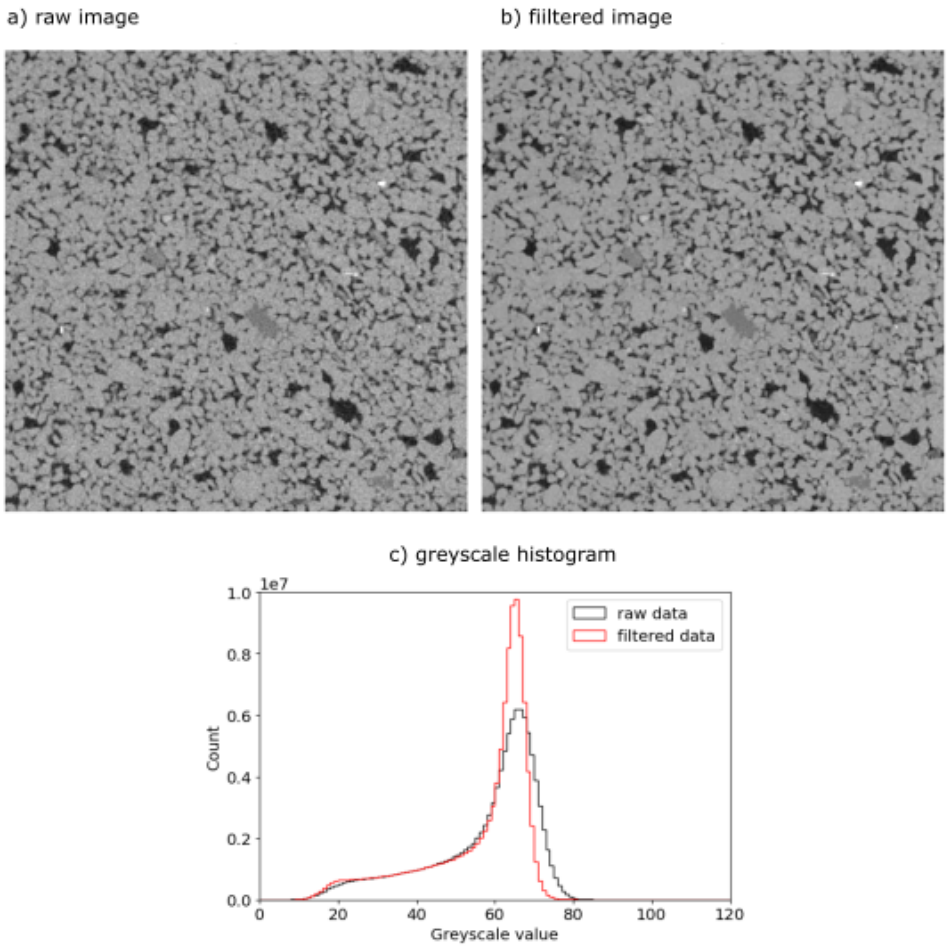

Figure 2. a) raw image, b) image filtered with a non-local means filter, and c) the change in the greyscale values histogram caused by the filtering.

The aim is to have the maximum amount of filtering while maintaining boundaries. The parameters that can be varied are fast_mode, which, if set to true, uses uniform spatial weighting on the patches, instead of a spatial Gaussian weighting. The noise standard deviation is given in sigma, with an additional function estimate_sigma used to es-

timate the correct value of sigma. The patch size and search area are given by patch_size and patch_distance, respectively. The patch size, and search area heavily control the run time of the filtering function.

The best filtering for this data set is fast_mode set to true, sigma set to 3 times the estimated sigma, a patch size of 3, and a patch distance of 6. This is shown in Figure 2. By parallel processing (running a number of patches at the same time), the image filtering time for a $1400 \times 1400 \times 600$ voxel image reduces from just over 1 hr to under 10 mins. We implement the non-local means filtering with the function nlm_denoise. Here, the patch size and distance can be changed, but the other parameters are set, as it is our recommendation to users to only change these parameters. Increasing the patch size has little impact on image quality for our images (see Figure 3a), but run time is proportional to patch size, so doubling increases the patch volume 4 times, thus the filtering takes 4 times as long. Changing sigma to 5 times the estimated sigma makes the images look smoother (see Figure 3c), but the grain boundaries begin to be influenced by the filtering process. An example is highlighted in the red circle in Figure 3c) and d).

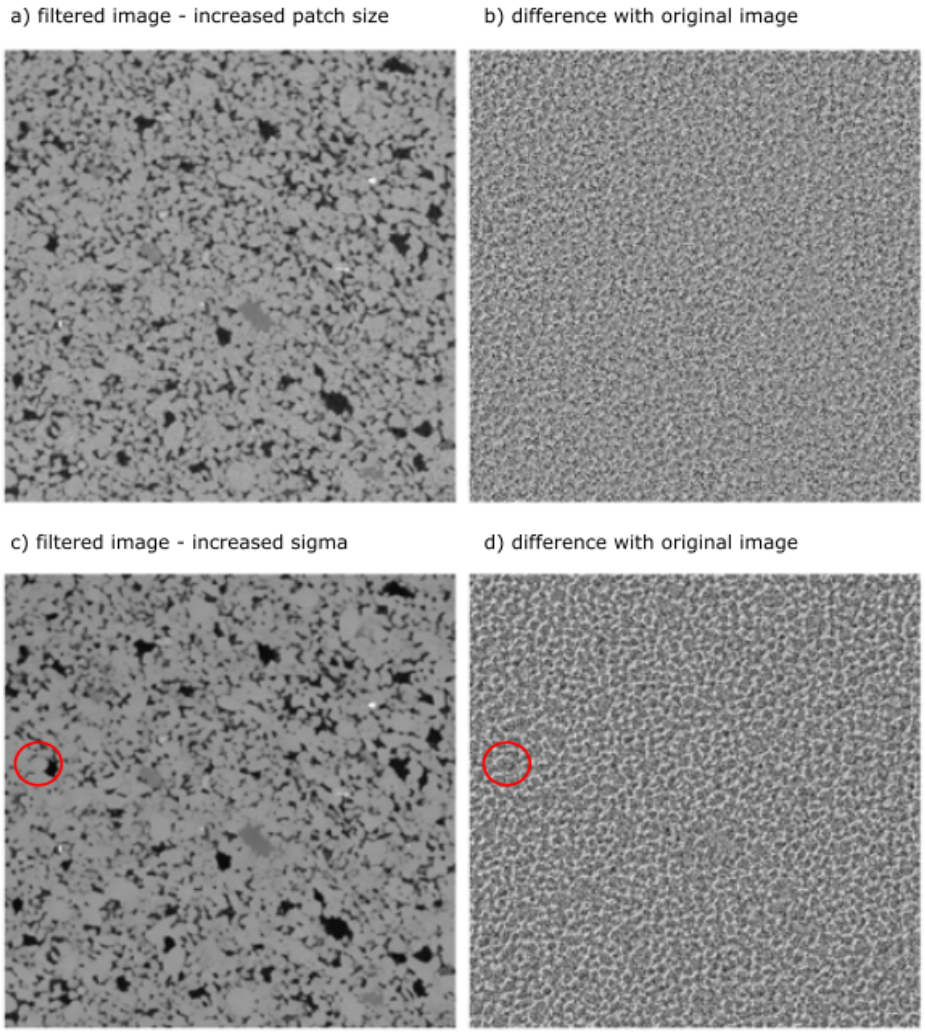

Figure 3. a) filtered image with an increased patch size, b) difference image of the filtered image in a) with the original image in Figure 2 a), c) filtered image with sigma doubled, and d) difference image of the filtered image in c) with the original image.

Other filtering procedures can be added here, if needed. For example, removing ring artefacts. However, a lot of these features are removed in the reconstruction, if the reconstruction parameters are selected correctly (Kaestner et al., 2008; Münch et al., 2009). As a result, we do not discuss them in the image processing workflow presented in this work.

3.2 Merging of sections

If multiple scans were taken to capture the entire pore space, the images must be merged. This can be done prior to segmentation if the full volume can be processed in one iteration. For a machine with 32GB ram, the maximum volume that could be processed using our workflow was 1400×1400×700 voxels. If the final image is larger than this, the segmented images can also be merged. If this is the case, then greyscale values must be consistent when segmenting. In utils.preprocess, prior to segmentation the input image is normalised to the maximum and minimum values in the input image. If the maximum and minimum greyscale value changes for the differ sections, this should be overwritten, with the global minimum and maximum used instead.

For merging, slices are compared until identical slices are found. If merging the segmented scans, there can be some variation caused by non-local means filtering at the edges. To overcome this, there should be around 100 slices overlap between sections that will be merged. If small movements occur between scans, then merging will fail e.g. a grain moving. Small spots, within the error of the segmentation should be removed, and the minimum size is set to 4 pixels in our case. This number can be increased, but should be done with caution. As merging is dependent on the number of sections to be merged, it is not put in function form. An example of merging is provided in the script flow_segmentation_3D as an example for users to adapt.

3.3 Watershed segmentation

The pore space of the rock sample is typically darker than the surrounding rock grains. However, there is overlap in the lightest regions of the pore space, and the darkest regions of the rock grains, leading to some overlap in greyscale values (see Figure 2c). As a result, a simple thresholding cannot be used to segment the pore space. Instead we use a watershed segmentation that looks at greyscale values, and gradients within the greyscale distribution.

For the function phase_segmentation_adapted_watershed the user inputs only one value. This is the value, below which, only pore space exists. The value, above which, only grains exist is calculated from the histogram. This is because, for most applications in subsurface porous media, the porosity is less than 30% of the total image, and so while a peak does not always exist in the greyscale histogram for the pore space, there is a peak associated to the rock grains, which make up the majority of the voxels in the image. A Gaussian distribution is fitted through this to get the threshold value for the grains.

Small spots are removed at the end of the segmentation to remove noise. Small spots, below 4 pixels in size are removed (note this is the same value used in the merging). These features are too small to be accurately analyzed, as they are close to the image resolution. The final segmentation of the pore space is shown in Figure 4 a).

3.4 Case study of binning 1 vs binning 2

Here, we look at the role of resolution on the segmentation of the pore space. We have two identical images of the pore space of a Bentheimer sandstone sample, except in one instance the binning of the images is 1, and in the other the binning is 2. The segmentation of the binning 2 example is shown in Figure 4. The segmentation of the bin-

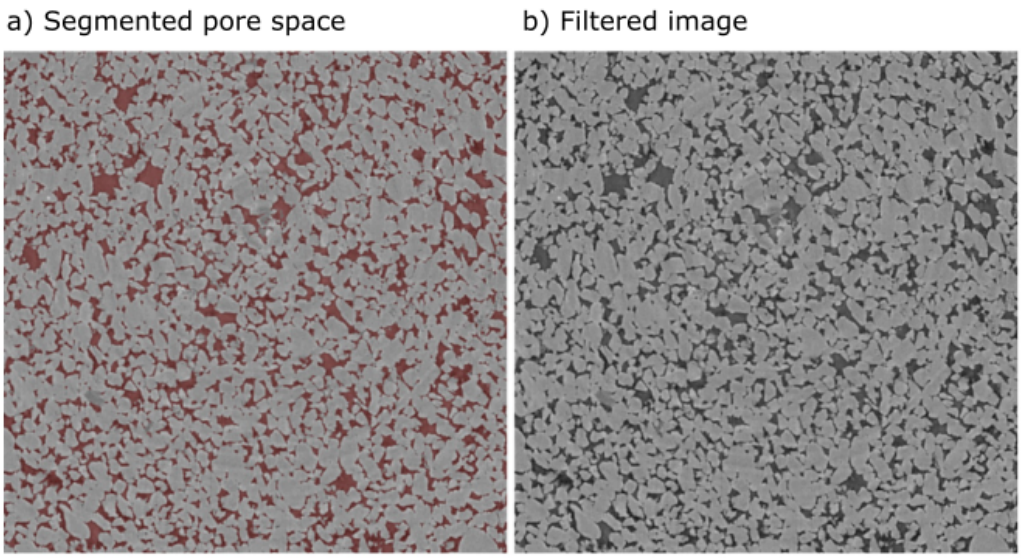

Figure 4. a) the segmented pore space overlain on the filtered image, and b) the filtered image.

ning 1 example is shown in Figure 5. Binning aims to reduce noise, but at the expense of image resolution, so the binning 2 image has a resolution of $20\mu m$ while the binning 1 image has a resolution of $10\mu m$. In this example, we take a small subvolume of the pore space: $1400\times1400\times100$ voxels for the binning 2 case, and $2800\times2800\times200$ voxels for the binning 1 case, so the same volume of sample was analyzed. The segmentation of the binning 1 image takes 6 times longer to run, and the images take up 4 times more memory. Thus the binning 2 images are easier to process, but important information may be lost in the binning process. However, the increase in resolution in the binning 1 case makes two distinct peaks in the greyscale histogram in Figure 5c). There is still overlap in the histograms, so watershed segmentation is still required to segment the pore space.

The porosity for the binning 2 image is 0.138, whereas it is 0.142 for the binning 1 image, a difference of 3%. There is a 20% difference in the connectivity of the pore space, calculated by the number of disconnected regions. These regions are connected via porosity below the resolution of the images, as no region remains filled with gas after brine is injected into the sample, thus all regions of the pore space must be connected to the inlet. This suggests that the increase in resolution picks up smaller connections in the pore space. The influence of binning on the connectivity of the non-wetting phase, is explore in the next section. As the non-wetting phase is more robust to image processing because it occupies the largest pores, it is a more important metric than the pore space connectivity. However, one should be mindful of missing connections when calculating absolute permeability from images, instead of measuring it directly on the sample using a pressure transducer.

4 Segmentation of Flow Images

4.1 Filtering using a non-local means filter

All flow images are filtered using the same non-local means filter as used in the segmentation of the pore space: nlm_denoise. This is done prior to registration. An example of the filtering is shown in Figure 6.

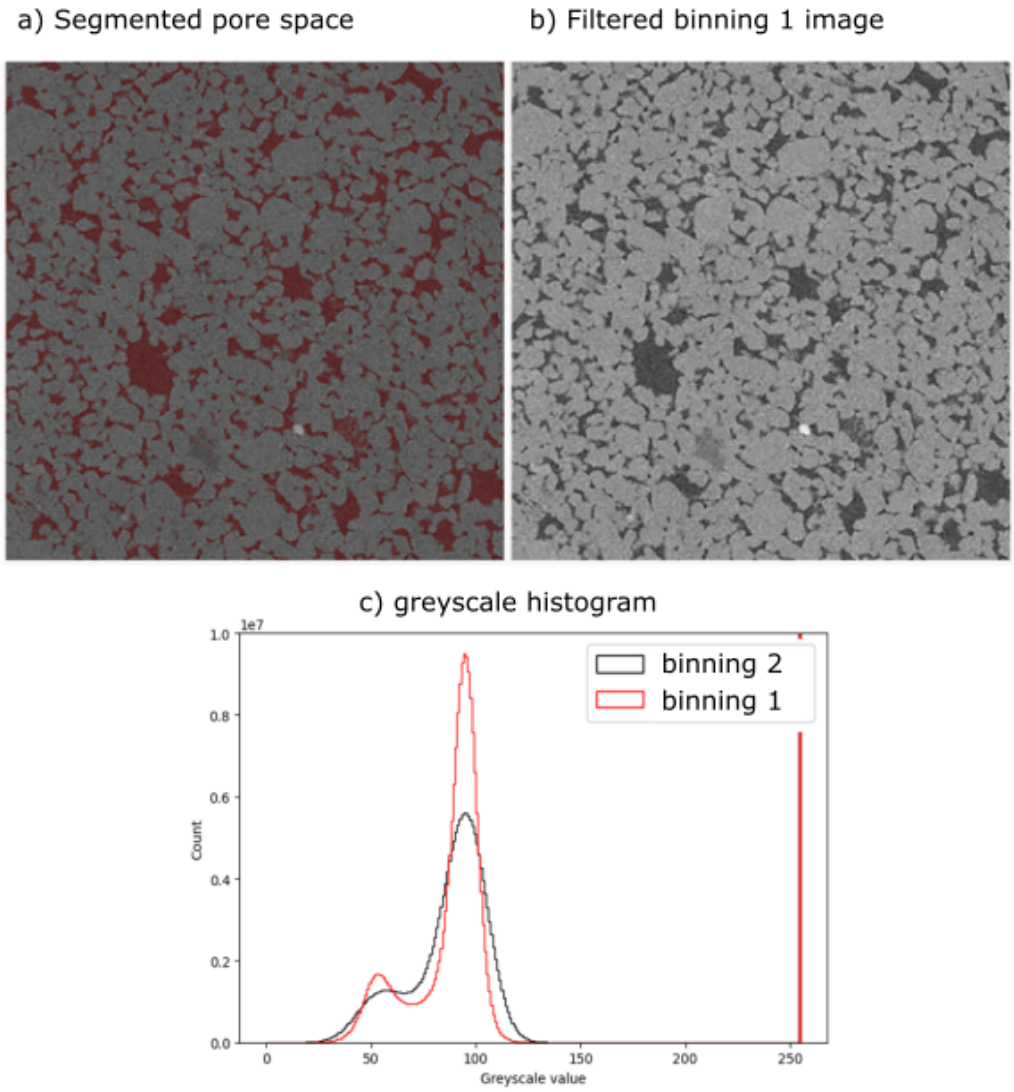

Figure 5. a) the segmented pore space overlain on the filtered binning 1 image, b) the filtered binning 1 image, and c) the greyscale histograms for the binning 1 and binning 2 images.

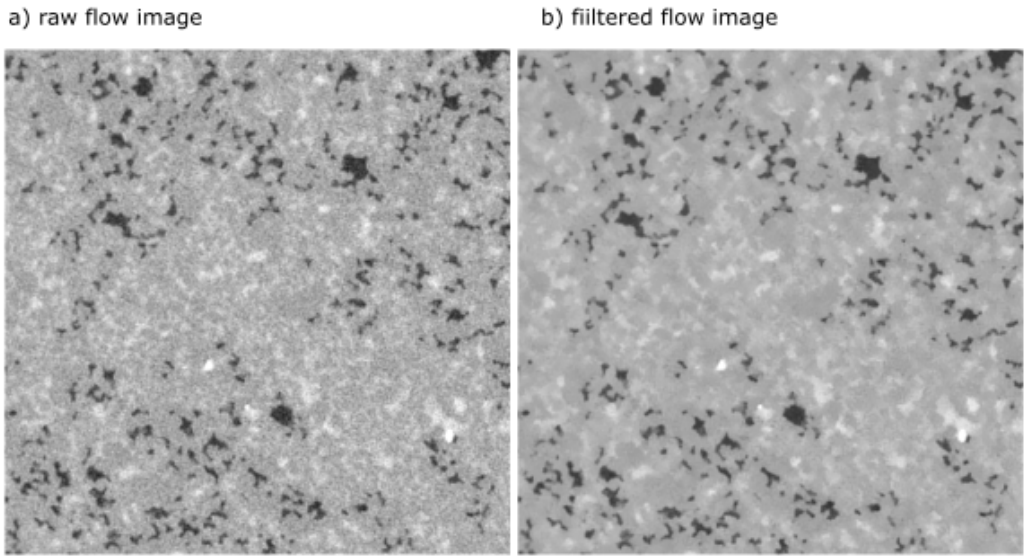

Figure 6. a) raw flow image b) the filtered flow image.

4.2 Registering to the dry scan

The flow images are registered to the initial image used for the segmentation of the pore space. This is necessary because small movement can occur during scanning. Without correcting for these, the segmentation of the fluids will be unsuccessful. The registration process is shown in Figure 7. The same slice is shown in Figure 7. Without registering, the masking of the flow image with the segmented pore space later in the segmentation of the flow scan would led to erroneous results, an example of this is highlighted by the red circle in Figure7.

To minimise the computational expense of the registration, we advise runner the registration of the flow images to a smaller subvolume, of the entire cross section of the core, and apply the registration to the whole image. In flow_segmentation_3D a subvolume of 50 slices in the z-direction, but the entire cross section, was used for the registration. The wet scan is noisier than the flow images, because the brine is more attenuating than the gas. It is advisable to register the image of a subvolume with a key feature (such as an inclusion), and then apply the registration to the entire volume. In our example, the registration is a simple translation. The script would need to be adapted if there is a shear movement, with re-sampling of the axes afterwards, if shear movement occurs.

4.3 Segmenting gas

The gas is segmented by subtracting the filtered, registered flow image from the filtered, registered brine scan. This leaves only the location of the gas, which is then segmented using a simple threshold. Post processing is carried out by removing small objects (smaller than 4 pixels) and filling in small holes (smaller than 4 pixels). The gas is then masked by the segmented pore space. This is all done in the script flow_segmentation_3D. An example of the gas segmentation is shown in Figure 8b).

The quality of the registration is evident if the gas saturation changes massively when the gas is masked by the segmented pore space. The quality of the registration can

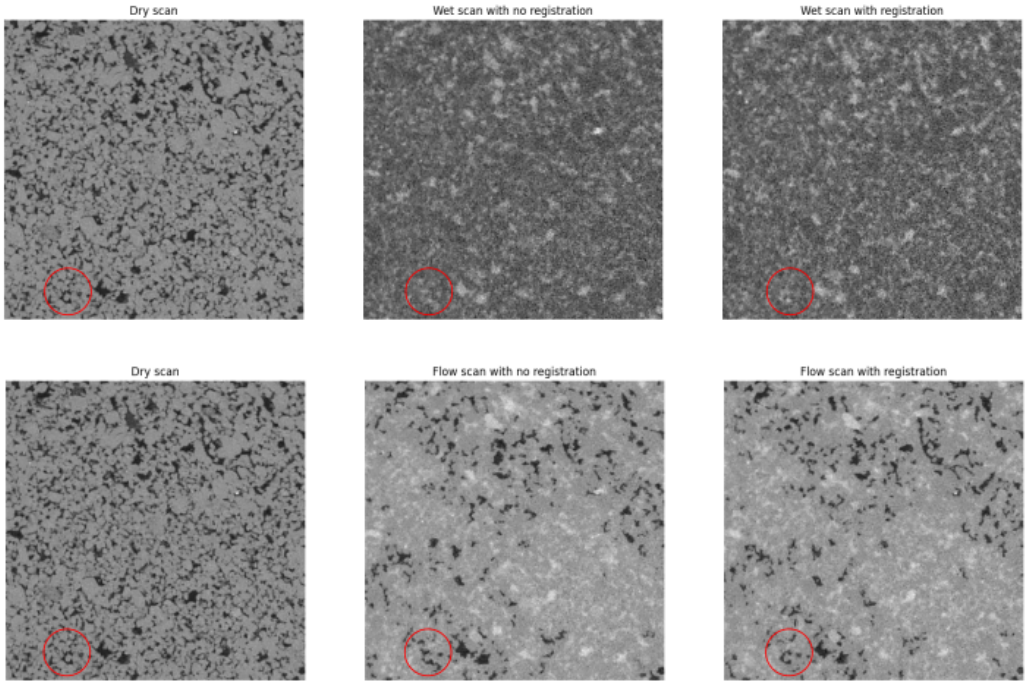

Figure 7. The impact of registering the wet scan (image with just the wetting phase present) and the flow scan (image with both phases present) with the high quality dry scan.

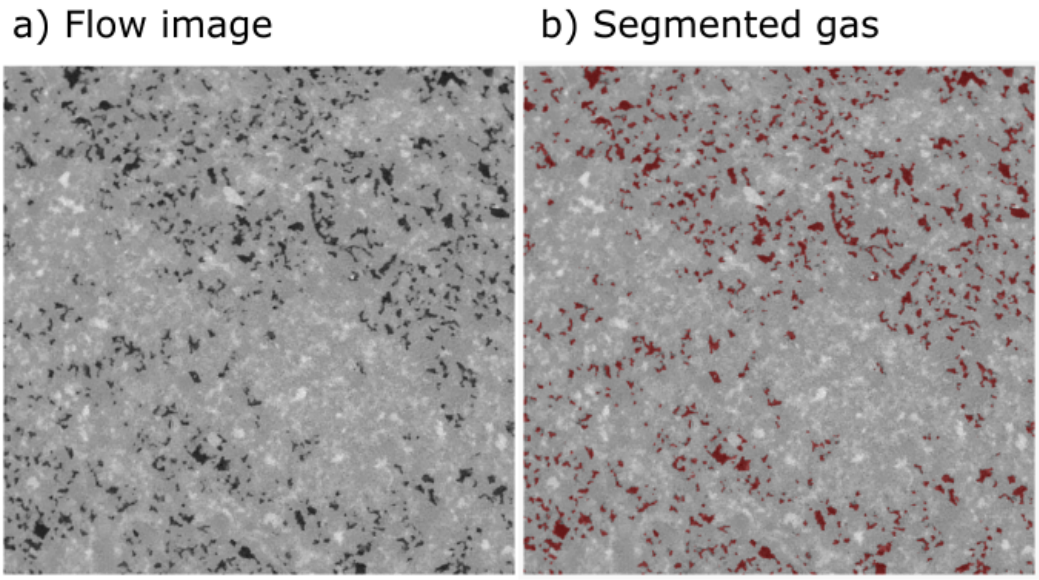

Figure 8. a) the flow image, and b) the segmented gas (red) overlain on the flow image.

be viewed for a single slice with utils.sanity_check, or for many slices with the interactive widget.

4.4 Segmenting water

The location of the water is calculated by assigning all locations of the pore space designated as gas, as water. This is a valid assumption for two-phase flow.

We now have the segmented image, with different binary numbers assigned to the different phases. For our script, flow_segmentation_3D, the rock grains are assigned 3, the gas is assigned 2, and the water is assigned 1. Alternatively the gas phase can be saved independently as a binary file, and the water calculated only when needed. Saving as a binary file with just the gas does reduce the memory required for the image, which is beneficial when sending data to other groups.

5 Conclusions

We demonstrate an effective, open-source workflow for processing multi-phase flow through porous media experiments. The workflow contains no machine learning tools. While machine learning tools can be consistent and fast, the output is unpredictable if the data falls outside of the distribution of the training images. Typically the training images are hand labelled, which is extremely time consuming, and depends on the user. Machine learning has been shown to be more consistent on noisy data, but its performance is similar to an algorithmic workflow with filtered images (Garfi et al., 2020).

The approach presented in this work could be expanded as an input for machine learning models, removing the time-consuming hand labelling required to train AI models. There is also the benefit of a rules-based approach not being a "black box", like in the case of machine learning, especially in the absence of a ground truth. Thus this approach can also be used as a standalone method for segmenting.

6 Data availability

The code described in this manuscript is available on GitHub: `https://github.com/cspurin/image_processing`.

7 Acknowledgements

Catherine Spurin and Hamdi Tchelepi acknowledge support from the GeoCquest consortium. Sharon Ellman is a PhD Fellow with the Research Foundation – Flanders (FWO) and acknowledges its support under grant 1182822N. T. Bultreys holds a senior postdoctoral fellowship from the Research Foundation-Flanders (FWO) under Grant No. 12X0922N. This research also received funding from the Research Foundation–Flanders under grant G051418N, G004820N and the UGent BOF funding for the Centre of Expertise UGCT (BOF.EXP.2017.0007). We also wish to thank Griffin Chure, for his useful tutorials on the python sci-kit library.

References

Arganda-Carreras, I., Kaynig, V., Rueden, C., Eliceiri, K. W., Schindelin, J., Cardona, A., & Sebastian Seung, H. (2017). Trainable weka segmentation: a machine learning tool for microscopy pixel classification. *Bioinformatics*, *33*(15), 2424–2426.

Berg, S., Ott, H., Klapp, S. A., Schwing, A., Neiteler, R., Brussee, N., ... others (2013). Real-time 3d imaging of haines jumps in porous media flow. *Proceed-*

ings of the National Academy of Sciences, *110*(10), 3755–3759.

Blunt, M. J. (2017). *Multiphase flow in permeable media: A pore-scale perspective*. Cambridge university press.

Buades, A., Coll, B., & Morel, J.-M. (2011). Non-local means denoising. *Image Processing On Line*, *1*, 208–212.

Bultreys, T., Boone, M. A., Boone, M. N., De Schryver, T., Masschaele, B., Van Hoorebeke, L., & Cnudde, V. (2016). Fast laboratory-based micro-computed tomography for pore-scale research: Illustrative experiments and perspectives on the future. *Advances in water resources*, *95*, 341–351.

Bultreys, T., Van Offenwert, S., Goethals, W., Boone, M. N., Aelterman, J., & Cnudde, V. (2022). X-ray tomographic micro-particle velocimetry in porous media. *Physics of Fluids*, *34*(4), 042008.

Garfi, G., John, C. M., Berg, S., & Krevor, S. (2020). The sensitivity of estimates of multiphase fluid and solid properties of porous rocks to image processing. *Transport in Porous Media*, *131*(3), 985–1005.

Garing, C., de Chalendar, J. A., Voltolini, M., Ajo-Franklin, J. B., & Benson, S. M. (2017). Pore-scale capillary pressure analysis using multi-scale x-ray micromotography. *Advances in Water Resources*, *104*, 223–241.

Kaestner, A., Lehmann, E., & Stampanoni, M. (2008). Imaging and image processing in porous media research. *Advances in Water Resources*, *31*(9), 1174–1187.

Mascini, A., Boone, M., Van Offenwert, S., Wang, S., Cnudde, V., & Bultreys, T. (2021). Fluid invasion dynamics in porous media with complex wettability and connectivity. *Geophysical Research Letters*, *48*(22), e2021GL095185.

Münch, B., Trtik, P., Marone, F., & Stampanoni, M. (2009). Stripe and ring artifact removal with combined wavelet—fourier filtering. *Optics express*, *17*(10), 8567–8591.

Scanziani, A., Alhosani, A., Lin, Q., Spurin, C., Garfi, G., Blunt, M. J., & Bijeljic, B. (2020). In situ characterization of three-phase flow in mixed-wet porous media using synchrotron imaging. *Water Resources Research*, *56*(9), e2020WR027873.

Spurin, C., Bultreys, T., Rücker, M., Garfi, G., Schlepütz, C. M., Novak, V., ... Krevor, S. (2020). Real-time imaging reveals distinct pore-scale dynamics during transient and equilibrium subsurface multiphase flow. *Water Resources Research*, *56*(12), e2020WR028287.

Wildenschild, D., & Sheppard, A. P. (2013). X-ray imaging and analysis techniques for quantifying pore-scale structure and processes in subsurface porous medium systems. *Advances in Water resources*, *51*, 217–246.

Zhang, Y., Bijeljic, B., Gao, Y., Goodarzi, S., Foroughi, S., & Blunt, M. J. (2023). Pore-scale observations of hydrogen trapping and migration in porous rock: Demonstrating the effect of ostwald ripening. *Geophysical Research Letters*, *50*(7), e2022GL102383.

Zhou, X.-H., McClure, J. E., Chen, C., & Xiao, H. (2022). Neural network–based pore flow field prediction in porous media using super resolution. *Physical Review Fluids*, *7*(7), 074302.